J. Fluid Mech. (1997), *vol.* 350, *pp.* 209–229. Printed in the United Kingdom

Convection in a rotating cylindrical annulus. Part 4. Modulations and transition to chaos at low Prandtl numbers

By J. HERRMANN AND F. H. BUSSE

Institute of Physics, University of Bayreuth, D-95440 Bayreuth, Germany

(Received 9 October 1996 and in revised form 18 April 1997)

Thermal Rossby waves driven by centrifugal buoyancy in a rotating cylindrical fluid gap become unstable right at the onset of convection when the Prandtl number is small. The Benjamin–Feir–Newell instability leads to modulated thermal Rossby waves which can also be described by a generalized Ginzburg–Landau equation. A resonance instability occurs at a finite distance in Rayleigh number from the neutral curve. It leads to two independent wave patterns propagating past each other and finally gives rise to vacillations of the amplitude of convection. Most of these features can be described to a good approximation by a system of three coupled amplitude equations. Time integrations based on a Galerkin expansion show transitions to chaotic convection at higher Rayleigh numbers.

1. Introduction

Thermal convection driven by centrifugal buoyancy in the fluid gap between two corotating coaxial cylinders kept at different temperatures has long been a subject of dual interest. On the one hand this system offers the simplest example of buoyancy-driven dynamics with a finite angle between the vectors of gravity and rotation. This situation is encountered in the case of convection in planets and in stars where rotation can play a dominant role. In fact, through the introduction of symmetric conical boundaries at the ends of the annular gap, the asymptotic theory for the onset of convection at high rotation rates becomes identical to that applicable in the case of self-gravitating rotating spheres (Busse 1970). The other reason for the study of the cylindrical annulus is the interesting nonlinear dynamics exhibited by the system. Sequences of bifurcations lead from the onset of symmetric thermal Rossby waves to realization of mean flow convection within a relatively small range of the Rayleigh numbers. The β-plane effect introduced by the variation of height of the annular gap with distance from the axis is responsible for dramatic differences of the system in comparison to a Rayleigh–Bénard convection layer. But in contrast to the latter, the dynamics can be described without explicit consideration of the dependence on the third coordinate in the direction of the axis of rotation. Various types of solutions have been explored in three previous papers (Busse & Or 1986; Or & Busse 1987; Schnaubelt & Busse 1992) and several others (Brummell & Hart 1993; Or & Herrmann 1995). But the case of a low-Prandtl-number fluid has received insufficient attention.

The reduction of the system to two spatial coordinates induced by the constraint of rotation becomes especially advantageous for low Prandtl numbers where new dynamical features must be expected. For a certain range of the Prandtl number P

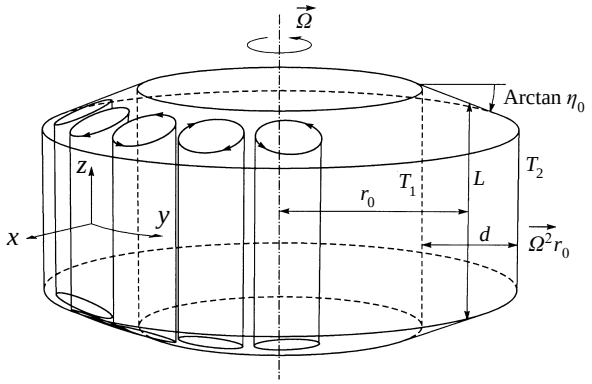

FIGURE 1. Geometrical configuration of the rotating cylindrical annulus.

all spatially periodic solutions (with a period length less than the circumference of the annulus) become unstable and a considerable numerical effort is required for an adequate description of the dynamics as will become apparent in later sections of this paper. Some of the features can be described through the use of complex Ginzburg–Landau equations (CGLE) and modifications thereof. But the full numerical solutions of the basic equations is necessary to delimit the range of applicability of the simpler equations.

The plan of this paper is as follows. In §2 a brief outline is given of the basic equations and methods for their solution. Thermal Rossby waves and their stability regions at low Prandtl numbers are discussed in §3. In the following section the sideband mechanisms of instability are analysed in more detail through the consideration of a generalized complex Ginzburg–Landau equation, while the resonance mechanism of instability is treated in the weakly nonlinear limit in §5. Some of the time-periodic, aperiodic and chaotic solutions introduced by the instabilities are discussed in §§6 and 7 for the cases of the sideband and the resonance mechanism, respectively. The paper closes with a concluding section where open problems are also mentioned.

2. Mathematical formulation of the problem

We consider the problem of convection in a cylindrical annulus rotating with the angular velocity Ω as shown in figure 1. The basic state of pure conduction is unstable owing to centrifugal buoyancy if the temperature T_2 of the outer cylinder exceeds the temperature T_1 of the inner cylinder by a sufficient amount. We neglect gravity which in a laboratory experiment will be directed parallel to the vertical axis of rotation. We shall use the small-gap approximation which allows us to use a Cartesian system of coordinates as indicated in the figure. The unit vector in the z-direction parallel to the axis of rotation will be denoted by $\boldsymbol{k}$. Using the gap width d as length scale, d^2/ν as time scale where ν is the kinematic viscosity of the fluid, and $(T_2 - T_1)P$ as temperature scale, we can write the equation of motion for the stream function ψ and the heat equation for the deviation Θ from the static temperature distribution in dimensionless form

$$\left(\frac{\partial}{\partial t} + \frac{\partial}{\partial y}\psi\frac{\partial}{\partial x} - \frac{\partial}{\partial x}\psi\frac{\partial}{\partial y} - \Delta_2\right)\Delta_2\psi - \eta\frac{\partial}{\partial y}\psi = -R\frac{\partial}{\partial y}\Theta, \tag{2.1a}$$

$$P\left(\frac{\partial}{\partial t} + \frac{\partial}{\partial y}\psi\frac{\partial}{\partial x} - \frac{\partial}{\partial x}\psi\frac{\partial}{\partial y}\right)\Theta - \Delta_2\Theta = -\frac{\partial}{\partial y}\psi, \tag{2.1b}$$

where Δ_2 denotes the two-dimensional Laplacian, $\Delta_2 = \partial^2/\partial x^2 + \partial^2/\partial y^2$, and Rayleigh number R, Prandtl number P and the rotation parameter η are defined by

$$R = \frac{\gamma(T_2 - T_1)\Omega^2 r_0 d^3}{\nu\kappa}, \quad P = \frac{\nu}{\kappa}, \quad \eta = \frac{4\eta_0 \Omega d^3}{\nu L}. \tag{2.2}$$

In these expressions γ, κ, r_0 and L denote the thermal expansivity, the thermal diffusivity, the mean radius of the annulus and its height, respectively.

For detailed derivations of (2.1) we refer to previous papers (Busse 1970, 1986) in which it has been demonstrated that the deviations from the two-dimensional velocity field $\boldsymbol{v} = \nabla\psi \times \boldsymbol{k}$ caused by the conical boundaries give rise to the term proportional to η in (2.1*a*). Without this term equations (2.1) are identical to those describing two-dimensional convection in a Rayleigh–Bénard layer. The deviation from the form $\boldsymbol{v} = \nabla\psi \times \boldsymbol{k}$ of the velocity field is of order η_0 which is the tangent of the angle between the conical surfaces and the equatorial plane of the annulus. While η_0 is required to be small, the parameter η is finite and may become large since we are considering the limit of large rotation rates, $\Omega d^2 \nu^{-1} \gg 1$.

The conditions at the isothermal, stress-free cylindrical boundaries are expressed by

$$\psi = \frac{\partial^2}{\partial x^2}\psi = \Theta = 0 \quad \text{at} \quad x = \pm\tfrac{1}{2}. \tag{2.3}$$

Other boundary conditions such as for example no-slip cylindrical walls have been considered in previous analyses (Schnaubelt & Busse 1992) in order to correspond more closely to experimental observations. But usually the differences in boundary conditions introduce only quantitative changes in the properties of the solutions of the problem. One problem caused by stress-free conditions is that an arbitrary constant zonal flow can be added to the velocity field. But this arbitrariness is removed when conditions (2.3) are also applied for the y-independent part of ψ. Since ψ must assume the same value on both walls our rotating frame of reference is defined by the condition that the mean zonal flux vanishes at all times.

We shall obtain solutions of (2.1) together with conditions (2.3) by using the Galerkin method in which the dependent variables are expanded into complete systems of functions that satisfy all boundary conditions,

$$\psi = \sum_{l,n} (\hat{a}_{ln} \cos l\alpha(y - ct) + \check{a}_{ln} \sin l\alpha(y - ct)) \sin n\pi(x + \tfrac{1}{2}), \tag{2.4a}$$

$$\Theta = \sum_{l,n} (\hat{b}_{ln} \cos l\alpha(y - ct) + \check{b}_{ln} \sin l\alpha(y - ct)) \sin n\pi(x + \tfrac{1}{2}). \tag{2.4b}$$

After (2.4) have been introduced in (2.1) and the latter have been projected onto the space of the expansion functions, a system of nonlinear ordinary differential equations in time for the coefficients $\hat{a}_{ln}, \check{a}_{ln}, \hat{b}_{ln}, \check{b}_{ln}$ is obtained. We have introduced the phase velocity c in (2.4) since there is a subset of solutions for which the coefficients are independent of time when seen from a suitably drifting frame of reference. The symmetric thermal Rossby waves and the mean flow solutions belong to this subset of stationary solutions. In order to determine the drift rate c for these latter solutions we make use of the invariance of the problem with respect to translation in time and fix the phase of the solution such that $\check{a}_{11} = 0$. This condition provides an extra equation for the determination of c. For actual numerical solutions the infinite system of equations must be truncated. We shall neglect all coefficients and corresponding

equations with subscript l, n satisfying

$$l > N_l, \qquad n > N_n, \tag{2.5}$$

where N_l and N_n are integer numbers that can be adjusted such that relevant properties of the solution do not change if they are significantly increased. Typically $N_l = N_n = 7$ was used. But in the case of computations with a long periodicity interval in the y-direction N_l was increased up to 127.

The stability of stationary solutions of the form (2.4) with constant coefficients can be investigated through the imposition of infinitesimal disturbances,

$$\tilde{\psi} = \exp\{\mathrm{i}d(y - ct) + \sigma t\} \sum_{l,n} \tilde{a}_{ln} \exp\{\mathrm{i}l\alpha(y - ct)\} \sin n\pi(x + \tfrac{1}{2}), \tag{2.6a}$$

$$\tilde{\Theta} = \exp\{\mathrm{i}d(y - ct) + \sigma t\} \sum_{l,n} \tilde{b}_{ln} \exp\{\mathrm{i}l\alpha(y - ct)\} \sin n\pi(x + \tfrac{1}{2}), \tag{2.6b}$$

where the complex growth rate σ becomes the eigenvalue in the linear homogeneous system of equations for the unknowns $\tilde{a}_{ln}, \tilde{b}_{ln}$. For a given stationary solution with the parameters R, α, P, η the growth rate σ can be determined as a function of the Floquet wavenumber d. Whenever there exists a value of σ with positive real part σ_r, then the stationary solution is unstable. Otherwise it will be regarded as stable. In this fashion regions of stability in the (R, α)-plane have been determined for given values of P and η as we shall discuss in the following. Besides the Galerkin method we shall employ various methods for the analysis of the weakly nonlinear problem which we shall describe in §§4 and 5.

3. Thermal Rossby waves and their instabilities

The linearized version of (2.1) is solved by (2.4) when all terms except those corresponding to $l = n = 1$ are neglected. The dispersion relation for $c_0(\alpha)$ and the expression for the Rayleigh number are given by

$$c_0(\alpha) = \eta(1 + P)^{-1}(\pi^2 + \alpha^2)^{-1} \equiv -\omega_0(\alpha)/\alpha, \tag{3.1a}$$

$$R_0(\alpha) = (\pi^2 + \alpha^2)^3 \alpha^{-2} + \left(\frac{P\eta}{1 + P}\right)^2 (\pi^2 + \alpha^2)^{-1}. \tag{3.1b}$$

Thermal Rossby waves bifurcate supercritically at the neutral curve given by (3.1b) from the basic static state of the system. These solutions of the form (2.4) are characterized by the property that all coefficients with $l + n =$ odd vanish. For this reason these solutions are also called symmetric thermal Rossby waves. They correspond to ordinary convection rolls in the limit $\eta = 0$ when the relationship for Rayleigh–Bénard convection is recovered from (3.1b). When the stability of these solutions is investigated it is found that the disturbances of the form (2.6) separate into two classes: the even class for which coefficients with odd $l + n$ vanish and the odd class for which the opposite property holds. For simplicity we shall call the latter class the odd disturbances, while the former class will be called even disturbances.

A typical example of a stability region is shown in figure 2. The stability boundaries of thermal Rossby waves indicated in figure 2 are similar to those obtained at Prandtl numbers of order unity except that the mean flow instability is replaced by another instability called the resonance instability since it is always characterized by a finite value of d at which the real part σ_r of the growth rate reaches a maximum which

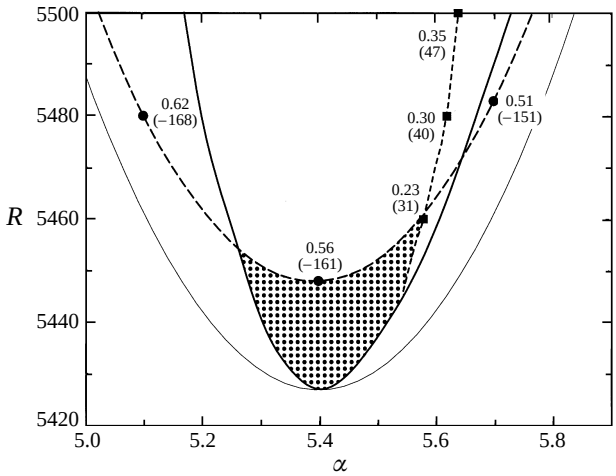

FIGURE 2. Stability boundaries of thermal Rossby waves for $P = 0.1, \eta = 4000$. Thermal Rossby waves are stable in the shaded region bounded by the parabola-shaped curve (thick solid line) which indicates the onset of the sideband instability with infinitesimal d, by the dashed curve indicating the onset of the resonance instability (long dashed line) and by the sideband instability with finite d (short dashed line). The preferred values of d for the latter two instabilities and the associated imaginary part σ_i of the growth rate (in brackets) are given at selected places on the stability boundaries. The thin parabolic curve indicates the neutral curve $R_0(\alpha)$.

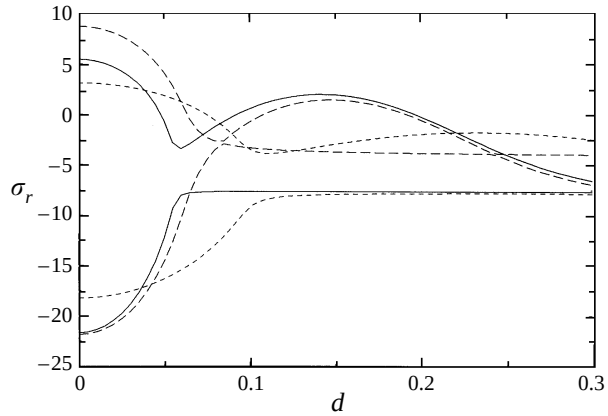

FIGURE 3. Real parts σ_r of the growth rate σ as a function of the Floquet wavenumber for the cases $P = 0.8, \alpha = 10.25, R = 45 \times 10^3, \eta = 4000$ (solid line), $P = 1.0, \alpha = 10.7, R = 54 \times 10^3, \eta = 4000$ (long dashed lines), and $P = 1.0, \alpha = 8.2, R = 22 \times 10^3, \eta = 2000$ (short dashed lines).

becomes rather sharp at low Prandtl numbers. Actually both instabilities correspond to two different maxima of the real part σ_r of the growth rate σ as function of d for odd disturbances as can be seen in figure 3. In the examples of this figure the growth rate of the mean flow disturbances at $d = 0$ with $\sigma_i = 0$ exceeds that of the second maximum. But at lower Prandtl numbers this situation is reversed. From the figure it is also evident that a switch-over of the eigenvalues takes place in the neighbourhood of $P = 1$ depending on the rotation parameter η. For higher Prandtl numbers the mean flow instability maximum and the resonance maximum thus correspond to different branches of the growth rate σ. Once the transition to mean flow convection has occurred the resonance instability manifests itself in a

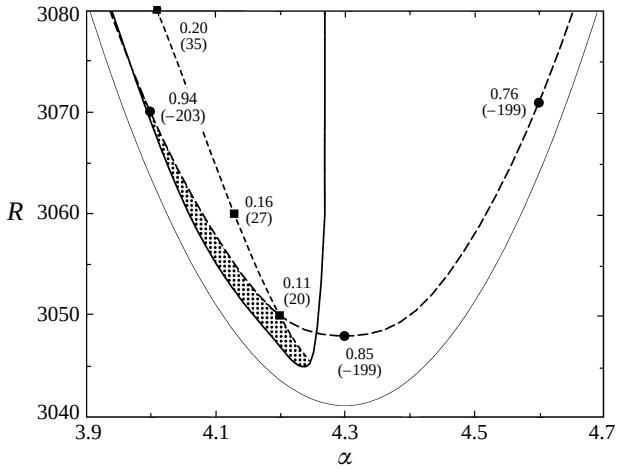

FIGURE 4. Same as figure 2, but in the case $P = 0.06, \eta = 4000$.

modified form as the vacillation instability known from earlier work (Or & Busse 1987; Schnaubelt & Busse 1992). But since the instability plays a different role at low Prandtl number and also because of the switch-over phenomenon we prefer to use the term resonance instability.

In addition to the odd disturbances, even disturbances restrict the region of stable thermal Rossby waves towards low and high wavenumber α. These sideband instabilities correspond to vanishingly small values of d in the neighbourhood of the critical Rayleigh number and are called Eckhaus instability in this case. But at higher Rayleigh number a second maximum of σ_r at a finite value of d develops and replaces the boundary corresponding to the infinitesimal value of d on the high-α side as indicated in figure 2.

The entire situation changes as the Prandtl number is decreased. Figure 4 shows a typical stability diagram for values P of order 0.05. The symmetric thermal Rossby waves are no longer stable in the neighbourhood of the neutral curve and their region of stability has been reduced to a small sliver paralleling the low-α branch of the neutral curve. The right-hand branch of the sideband instability with infinitesimal d becomes independent of R, while the branch corresponding to finite values of d has moved to the left and parallels the left-hand branch of the sideband instability. This rapid change of the sideband instability boundaries has been noted by Or (1990). But because of insufficient numerical resolution it was not recognized in that paper that the thermal Rossby waves become unstable near the critical Rayleigh number. The major part of the stability boundary towards higher values of R still corresponds to the modulation instability which was not considered by Or (1990). For lower values of η, this stability boundary moves to much higher values of R and just a small band of stable symmetric thermal Rossby waves remains paralleling the left-hand branch of the neutral curve. For even lower values of the Prandtl number the thin band of stability disappears entirely as can be seen in the paper of Or & Herrmann (1995).

Since the processes discussed here happen at small amplitudes of convection, it seems possible to describe them within weakly nonlinear theories. Accordingly we shall use two different approaches in §§4 and 5 for the description of the sideband instabilities and the resonance instability, respectively.

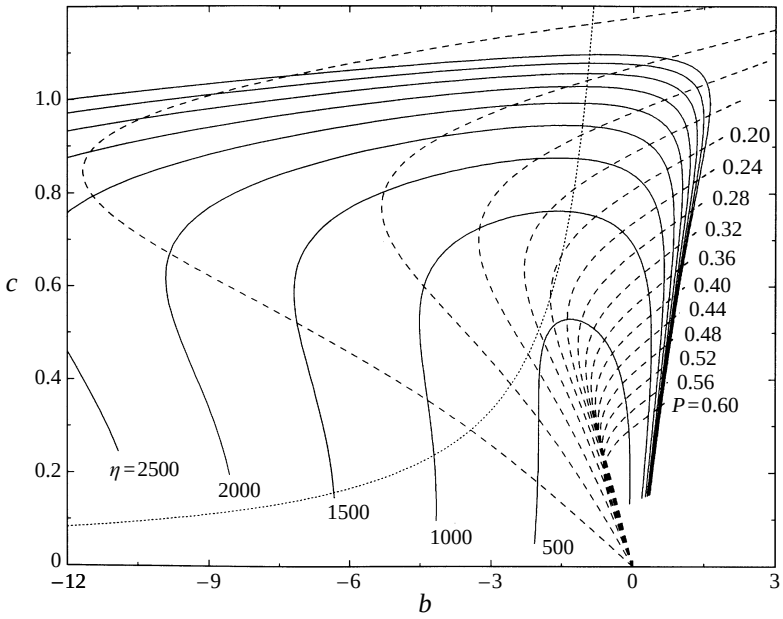

FIGURE 5. Dependence of coefficients b and c in the complex Ginzburg–Landau equation (4.1) on η and P. Stationary solutions are unstable to the left of the dotted line corresponding to criterion (4.2).

4. A generalized complex Ginzburg–Landau equation

The complex Ginzburg–Landau equation represents a universal description for large-scale variations of one-dimensional dynamical patterns. For a review we refer to the article by Cross & Hohenberg (1993). The equation is usually written in the form

$$\partial_T \hat{A} = \hat{A} + (1 + \mathrm{i}b)\partial_{YY}^2 \hat{A} - (1 + \mathrm{i}c)|\hat{A}|^2 \hat{A}, \tag{4.1}$$

where $\hat{A}$ represents the amplitude of the thermal Rossby wave scaled by $(R - R_c)$ which varies on the long scale Y in the y-direction and depends on the slow time scale T. It is well known that solutions with constant A corresponding to Rossby waves with the critical wavenumber α_c are unstable in the neighbourhood of the critical Rayleigh number R_c when the Newell criterion (Newell 1974)

$$1 + bc < 0 \tag{4.2}$$

is satisfied. As has already been discussed by Herrmann & Busse (1994) the instability of thermal Rossby waves at $R = R_c$ shown in figure 4 is described by the criterion (4.2). In figure 5 the parameters b and c are related to the parameters η and P of the thermal Rossby waves. In figure 6 the region in the (P, η)-plane for which thermal Rossby waves are unstable according to the criterion (4.2) at $R = R_c$ is outlined. It is of interest to note that at very small Prandtl numbers P the thermal Rossby waves regain their stability at $R = R_c$. Because of its symmetry with respect to $\alpha = \alpha_c$, (4.1) is clearly not suited to describe the asymmetric stability boundaries beyond the critical Rayleigh number. Asymmetric terms of higher order become important since the original prefactor of the cubic term is proportional to P^2 in the limit of small Prandtl numbers as can be seen from (4.4*d*) given below. Accordingly we consider

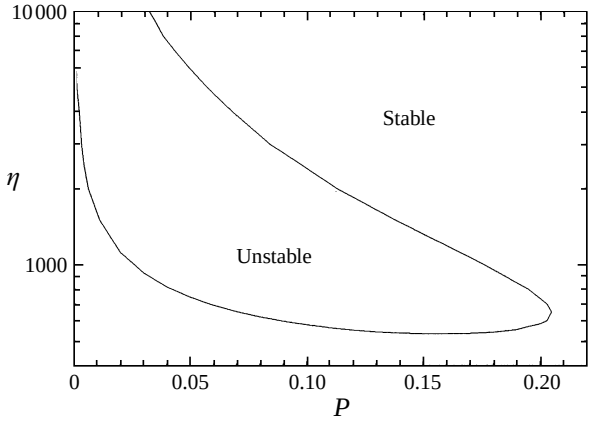

FIGURE 6. The region in the (P, η)-plane where thermal Rossby waves are unstable at the critical value R_c of the Rayleigh number based on the Newell criterion (4.2).

the following generalized complex Ginzburg–Landau equation (GCGLE):

$$\frac{\partial}{\partial t}A = s(R - R_c)A + \beta\frac{\partial^2}{\partial y^2}A - \delta|A|^2A + \gamma A\frac{\partial}{\partial y}|A|^2, \tag{4.3}$$

where the abbreviations

$$s = \frac{\partial}{\partial R}\sigma\,(\alpha, R)|_{\alpha_c, R_c} = \mathrm{i}\alpha_c\xi/\tau, \tag{4.4a}$$

$$\beta = -\frac{1}{2}\frac{\partial^2}{\partial\alpha^2}\sigma\,(\alpha, R)|_{\alpha_c, R_c} = (-\mathrm{i}\alpha_c c(\alpha_c) + 6\alpha_c^2 + 4\pi^2 - R_c\xi^2 - 2\mathrm{i}\alpha_c v_g)\tau^{-1}, \tag{4.4b}$$

$$v_g = -\frac{\partial}{\partial\alpha}\sigma_i\,(\alpha, R)|_{\alpha_c, R_c} = (-c(\alpha_c)\alpha_c^2 + \tfrac{1}{2}\eta - 2\mathrm{i}\alpha_c(\pi^2 + \alpha_c^2) - R_c\xi(1 - \mathrm{i}\alpha_c\xi))2\tau^{-1}, \tag{4.4c}$$

$$\delta = P^2\alpha_c^2 R_c\xi(\xi^* - \xi)/4\tau, \tag{4.4d}$$

$$\gamma = \mathrm{i}\alpha_c^3(3 - \alpha_c^2\pi^{-2})/8\tau + \ldots, \tag{4.4e}$$

$$\xi = -\mathrm{i}\alpha_c(\alpha_c^2 + \pi^2 - \mathrm{i}\alpha_c c(\alpha_c)P)^{-1}, \tag{4.4f}$$

$$\tau = \alpha_c^2 + \pi^2 - R_c\xi^2 P \tag{4.4g}$$

have been used. ξ^* denotes the complex conjugate of ξ. For γ the rather lengthy full expression has not been written explicitly. The terms not given in (4.4*e*) vanish in the limit $P \to 0$, however. Even though these terms make only a small contribution at low Prandtl numbers, they have been taken into account in the actual calculations. Equation (4.3) has been derived in the same way as the usual Ginzburg–Landau equation through the introduction of the slowly varying complex amplitude $A(y, t)$,

$$\psi(x, y, t) = (A(y, t)\exp\{\mathrm{i}\alpha_c(y - ct)\} + \text{c.c.})\sin\pi(x + \tfrac{1}{2}) + \text{h.o.t.}, \tag{4.5}$$

where c.c. indicates the complex conjugate and higher-order terms (h.o.t.) have not been denoted explicitly. But we have dispensed with the introduction of scaled variables in order to make solutions of (4.3) more directly comparable with the numerical results of the Galerkin method. Since $A(y, t)$ varies on a length scale of order A^{-1}, the last term of (4.3) is of fourth order. There are other terms of fourth order in addition

to this, but they have not been included since they vanish in the limit $P \to 0$ which is of primary interest.

In the analysis of sideband instabilities on the basis of the GCGLE we start with spatially periodic solutions of the form

$$A(y,t) = A_0 \exp\{\mathrm{i}qy + \mathrm{i}\mu t\}, \tag{4.6a}$$

with

$$|A_0|^2 = (s_r(R - R_c) - \beta_r q^2)/\delta_r, \tag{4.6b}$$

$$\mu = s_i(R - R_c) - \beta_i q^2 - \delta_i |A_0|^2, \tag{4.6c}$$

where the subscripts r, i refer to the real and imaginary parts, respectively. It is obvious from (4.6*b*) that the departure q of the wavenumber from the critical value α_c must be limited to small values when $R - R_c$ is a small positive number. The stability of (4.6) with respect to infinitesimal long-wave disturbances $\tilde{A}$ can be studied with the ansatz

$$A(y,t) = (A_0 + \tilde{A}(y,t)) \exp\{\mathrm{i}qy + \mathrm{i}\mu t\}, \tag{4.7}$$

where a real A_0 can be assumed without losing generality. The linearized equation for $\tilde{A}$ derived from (4.3) assumes the form

$$\frac{\partial}{\partial t}\tilde{A} = 2\mathrm{i}q\beta \frac{\partial}{\partial y}\tilde{A} + \beta \frac{\partial^2}{\partial y^2}\tilde{A} - A_0^2 \left(\delta - \gamma \frac{\partial}{\partial y}\right)(\tilde{A} + \tilde{A}^*), \tag{4.8}$$

which can be solved by a solution of the form

$$\tilde{A}(y,t) = a_1 \exp\{\mathrm{i}dy + \sigma t\} + a_2 \exp\{-\mathrm{i}dy + \sigma^* t\}. \tag{4.9}$$

The solvability condition for the two linear homogeneous equations for a_1 and a_2^* yields the following equation for σ:

$$\begin{aligned}\sigma^2 + 2\sigma(2\mathrm{i}q\beta_i d + \beta_r d^2 + (\delta_r - \mathrm{i}\gamma_r d)A_0^2) + |\,\beta\,|^2\, d^2(d^2 - 4q^2) \\ + (\beta(\delta^* - \mathrm{i}\gamma^* d)(2q + d) - \beta^*(\delta - \mathrm{i}\gamma d)(2q - d))A_0^2 d = 0.\end{aligned} \tag{4.10}$$

The wavenumber d in (4.9) has the same meaning as the Floquet wavenumber in the Galerkin representation (2.6). Indeed, a Floquet ansatz can be used in place of the ansatz (4.7), (4.9) which results in the same quadratic equation (4.10) for σ. For $d = 0$ this equation yields the solution $\sigma = 0$ corresponding to an infinitesimal shift of (4.6) in the y-direction. For small but finite values of d we obtain for $\sigma = \sigma_r + \mathrm{i}\sigma_i$

$$\sigma_r = d^2\{2q^2\beta_r^2 \,|\, \delta \,|^2\, A_0^{-2}/\delta_r - \beta_r\delta_r^2 - \beta_i\delta_i\delta_r - 2q\beta_r(\gamma_r\delta_i - \gamma_i\delta_r)\}\delta_r^{-2} + o(d^4), \tag{4.11a}$$

$$\sigma_i = 2q(\beta_r\delta_i\delta_r^{-1} - \beta_i) + o(d^3). \tag{4.11b}$$

Accordingly solutions of the form (4.6) are unstable for

$$\delta_r(\beta_r\delta_r + \beta_i\delta_i) + 2q\beta_r(\gamma_r\delta_i - \gamma_i\delta_r) < 0. \tag{4.12}$$

If this criterion is not satisfied they can be stable only if

$$R - R_c > \frac{\beta_r}{s_r} q^2 \left[1 + \frac{2\,|\,\delta\,|^2}{\delta_r^2 + \delta_i\delta_r\beta_i/\beta_r + 2q(\gamma_r\delta_i - \gamma_i\delta_r)}\right]. \tag{4.13}$$

Condition (4.12) implies that (4.6) is unstable for the critical wavenumber, $q = 0$, when $\beta_r\delta_r + \beta_i\delta_i < 0$ which is identical with the Newell criterion (4.2). Since the first

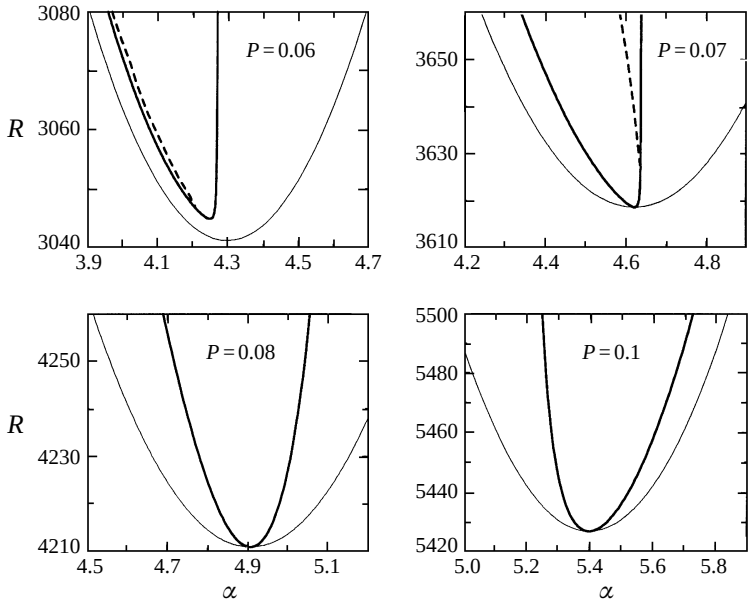

FIGURE 7. Sideband instability boundaries of thermal Rossby waves in the (R, α)-plane based on the GCGLE (4.2) in the case $\eta = 4000$ for different Prandtl numbers P as indicated. The boundaries corresponding to the onset of sideband disturbances with infinitesimal values of d are shown by thick lines, and the onset of instability corresponding to finite values of d is indicated by the dashed lines. Thermal Rossby waves are only stable to the left of the dashed lines in the upper plots. The thin parabolas indicate the neutral curve.

term in the wavy bracket of (4.11a) tends to zero with increasing Rayleigh number, the wavenumber

$$q_s = -\frac{\delta_r(\beta_r\delta_r + \beta_i\delta_i)}{2\beta_r(\gamma_r\delta_i - \gamma_i\delta_r)} \tag{4.14}$$

represents an asymptotic R-independent stability boundary. This boundary is quite apparent in the stability diagram of figure 4. It is also apparent in the set of stability diagrams of figure 7 where it can be seen that q_s moves to positive values with increasing Prandtl number P, then disappears as the denominator of (4.14) goes through zero and reappears at negative values in the case $P = 0.1$.

The stability boundaries of figure 7 agree remarkably well with those of the Galerkin computations. This agreement includes the sideband stability boundary corresponding to finite values of d which can be obtained from the evaluation of the full expression (4.10). Since the relevant values of d are only a few percent of α_c the GCGLE still provides a good approximation.

5. Amplitude equations for the resonance instability

The success in describing the sideband instabilities in the weakly nonlinear limit motivates us to try a similar description for the resonance instability. We start with the expansion in powers of the amplitude A_1 of a periodic symmetric thermal Rossby wave (Busse & Or 1986),

$$\psi(x, y, t) = A_1 \exp\{\mathrm{i}\alpha y + \mathrm{i}\omega t\} \sin \pi(x + \tfrac{1}{2}) + \text{c.c.} + \text{h.o.t.}, \tag{5.1a}$$

$$\Theta(x,y,t) = -\frac{\mathrm{i}A_1\alpha\sin\pi(x+\frac{1}{2})}{\pi^2+\alpha^2+\mathrm{i}\omega_1 P}\exp\{\mathrm{i}\alpha y+\mathrm{i}\omega t\}+\text{c.c.}$$
$$+\frac{P\alpha^2A_1^2(\pi^2+\alpha^2)/2\pi}{\omega_1^2P^2+(\pi^2+\alpha^2)^2}\sin 2\pi(x+\tfrac{1}{2})+\text{h.o.t.}, \tag{5.1b}$$

$$R = R_0(\alpha)(1+A_1^2P^2\frac{(\pi^2+\alpha^2)\alpha^2/2}{\omega_1^2P^2+(\pi^2+\alpha^2)^2}+\text{h.o.t.}), \tag{5.1c}$$

$$\omega = \omega_1+\text{h.o.t.}\quad\text{with}\quad \omega_1\equiv\omega_0(\alpha), \tag{5.1d}$$

where terms of order A_1^3 and higher (h.o.t.) have not been denoted explicitly. We superimpose an infinitesimal disturbance of the form

$$\tilde{\psi}(x,y,t) = \tilde{A}_2\exp\{\mathrm{i}dy+\mathrm{i}\omega_2 t+\sigma_2 t\}\sin\pi(x+\tfrac{1}{2})\quad\text{with}\quad \omega_2\equiv\omega_0(d), \tag{5.2}$$

i.e. we take into account only the term with $l=0$ and $n=1$ in (2.6*a*). The expression for the complex growth rate σ can be written in the form

$$\sigma_2 = \sigma_0(R,d)+b_{21}\mid A_1\mid^2 \tag{5.3}$$

where $\sigma_0(R,d)$ denotes the complex growth rate determined from the linear part of (2.1), i.e. $\sigma_0(R_0(\alpha),\alpha)\equiv\mathrm{i}\omega_0(\alpha)$. The coefficient b_{21} is given by a complex expression which simplifies in the limit of low Prandtl numbers to

$$b_{21}\to\frac{\pi^2(d^2-\alpha^2)}{4(d^2+\pi^2)}\left\{\frac{(\alpha+d)^2((\alpha-d)^2-\alpha^2+3\pi^2)}{(\sigma^{(2)}(R,d-\alpha)+\mathrm{i}(\omega_1-\omega_2))((\alpha-d)^2+4\pi^2)}\right.$$
$$\left.+\frac{(\alpha-d)^2((\alpha+d)^2-\alpha^2+3\pi^2)}{(\sigma^{(2)}(R,\alpha+d)-\mathrm{i}(\omega_1+\omega_2))((\alpha+d)^2+4\pi^2)}\right\}\ \text{for } P\to 0, \tag{5.4}$$

where $\sigma^{(2)}(R,\delta)$ denotes the complex growth rate of the mode proportional to $\exp\{\mathrm{i}\delta y\}\sin 2\pi(x+\frac{1}{2})$ based on the linear part of (2.1). In the limit of $P\to 0$ with ηP kept constant the real and imaginary parts of the function $\sigma^{(2)}(R,\delta)$ can be written down readily:

$$\left.\begin{aligned}\sigma_i^{(2)} &= \frac{-\delta\eta}{4\pi^2+\delta^2},\\ \sigma_r^{(2)} &= \left[R\delta^2-\frac{\delta^2\eta^2P^2}{4\pi^2+\delta^2}-(4\pi^2+\delta^2)^3\right]\left[(4\pi^2+\delta^2)^2+\frac{\delta^2\eta^2P^2}{(4\pi^2+\delta^2)^2}\right]^{-1},\end{aligned}\right\} \tag{5.5}$$

but at finite Prandtl numbers more complex expressions arise and real and imaginary parts of $\sigma^{(2)}$ can not easily be given separately. Because the frequencies in the denominators of (5.4) increase with η the second term on the right-hand side of (5.3) cannot compensate the usually negative contribution to the real part of the first term for large η. But in the case of a resonance at the wavenumber $d=d_0$,

$$\sigma_i^{(2)}(R,d_0-\alpha)+\omega_1-\omega_2 = 0, \tag{5.6}$$

positive real parts σ_{2r} do indeed become possible. Since we are assuming $0<d<\alpha$ the resonance given by (5.6) is the only one occurring in (5.4). The resonance also provides the justification for neglecting the disturbance

$$\tilde{\psi}\propto\exp\{\mathrm{i}(\alpha-d)y+\mathrm{i}\omega_3 t+\sigma t\}\sin\pi(x+\tfrac{1}{2})\quad\text{with}\quad\omega_3\equiv\omega_0(\alpha-d), \tag{5.7}$$

which together with the mode (5.2) forms a coupled system of disturbances and which is included in the sideband instability mechanisms discussed in the preceding section. But since there is only one resonating term (except in the special case $d_0=\alpha/2$ which

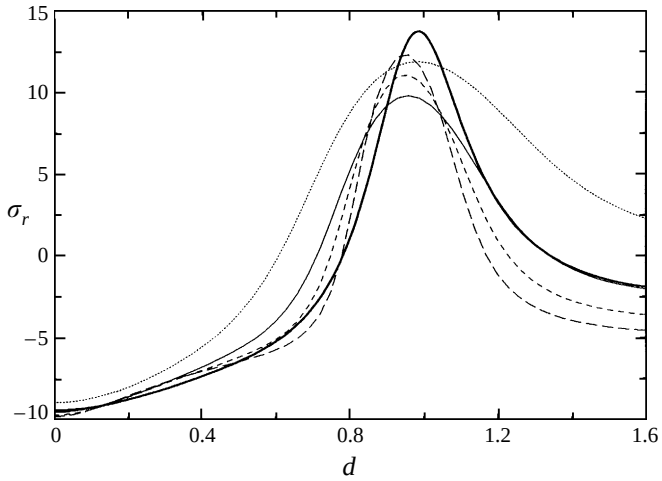

FIGURE 8. Real parts σ_r of the growth rate of the resonance instability as a function of d for $\alpha = 4.0, P = 0.05$ in the cases $\eta = 6000, R = 4255$ (long dashed line), $\eta = 5000, R = 3290$ (short dashed line), $\eta = 4000, R = 2500$ (thin solid line), $\eta = 3000, R = 1890$ (dotted line). For comparison σ_r based on the approximate expression (5.3) has been plotted (thick solid line) for the same parameter values as the long dashed line.

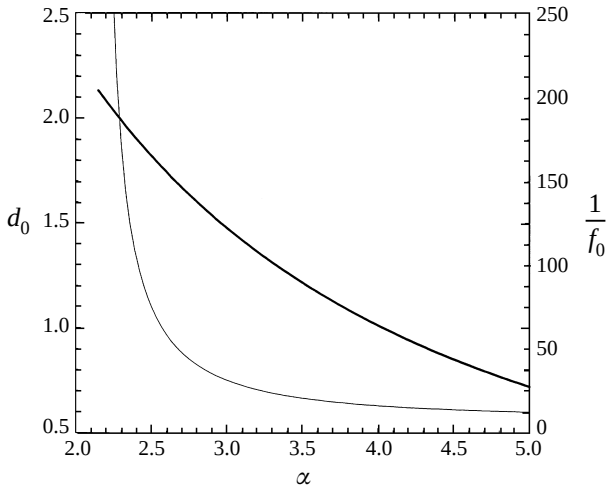

FIGURE 9. Resonance wavenumber d_0 (thick line) and coefficient f_0 (thin line, right ordinate) as a function of α in the case $P = 0$.

is not realized) the assumption of neglecting the part (5.7) of the growing disturbance is indeed justified.

The following properties of the resonance instability can be deduced:

(i) Since all terms involved in the resonance condition (5.6) are proportional to η, or nearly so at low values of P, the resonating disturbance wavenumber d_0 is independent of η as is borne out in figure 8 where the real part σ_r of the growth rate derived from the numerical stability analysis is plotted for different values of η. For comparison σ_r given by the approximate analytical expression (5.3) is also shown. The resonating wavenumber d_0 is plotted in figure 9 as a function of α for the case

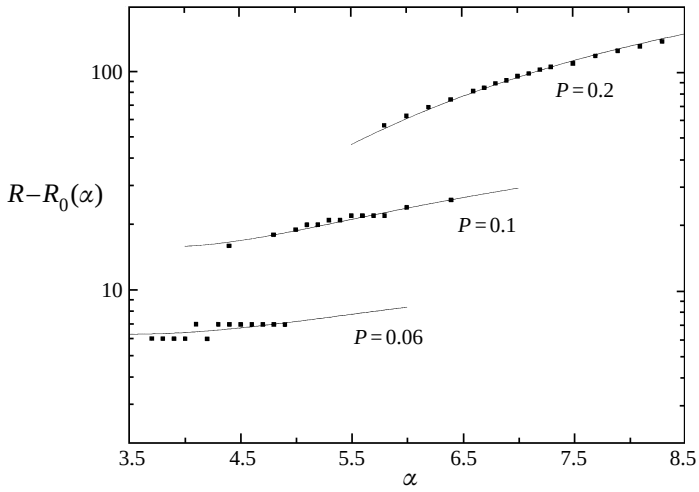

FIGURE 10. Rayleigh number R for the onset of the resonance instability in the case $\eta = 4000$ for three different Prandtl numbers as indicated. The analytical results (solid lines) are compared with the results of the numerical Galerkin method.

$P = 0$. Almost within the thickness of the line the expression derived from condition (5.6) agrees with the numerical results for small Prandtl number.

(ii) Expression (5.3) also allows us to compute the half-width of the resonance peak of σ_r,

$$b_{21r} \propto [(\sigma_r^{(2)}(R, \alpha - d_0))^2 + \eta^2 f_0^2 (d - d_0)^2]^{-1} \text{ for } \mid d - d_0 \mid \ll 1, \tag{5.8}$$

where the subscript r refers to the real part and f_0 is a constant independent of η. Expression (5.8) clearly describes the decrease of the width of the resonance peak with increasing η, which is also visible in the numerical data of figure 8. On the other hand the broadening of the resonance with decreasing η becomes so strong that the resonance is no longer clearly distinguished within the general sideband mechanism of instability for η of the order of 10^3. For this reason the resonance instability disappears in the stability diagram of figure 2 when η is changed from 4000 to 1000 (Herrmann 1996). Of course, the analytical expression (5.3) also ceases to provide a good approximation at such low values of η.

(iii) Since the real parts of the first term on the right-hand side of (5.3) increase approximately linearly with R and since the second term is proportional to $R - R_0(\alpha)$ according to (5.1c) we obtain the following approximate expression for the Rayleigh number R_R for the onset of the resonance instability above the neutral curve $R = R_0(\alpha)$:

$$R_R(\alpha) - R_0(\alpha) = -\sigma_{0r}(R_0(\alpha), d_0) \left[\frac{b_{21}}{P^2(\pi^2 + \alpha^2)^2} + \frac{1}{2} \left. \frac{\partial \sigma_0}{\partial R} \right|_{R_0, d_0} + \text{c.c.} \right]^{-1}. \tag{5.9}$$

The comparison of this analytical expression with the numerical results in figure 10 indicates again the remarkably good agreement between the two approaches.

In discussing the resonance instability we have emphasized the low-Prandtl-number regime where this instability occurs at relatively low Rayleigh numbers. The resonance mechanism operates at higher values of P as well, but the amplitude of the basic symmetric thermal Rossby wave decreases in proportion to $1/P$ for a fixed

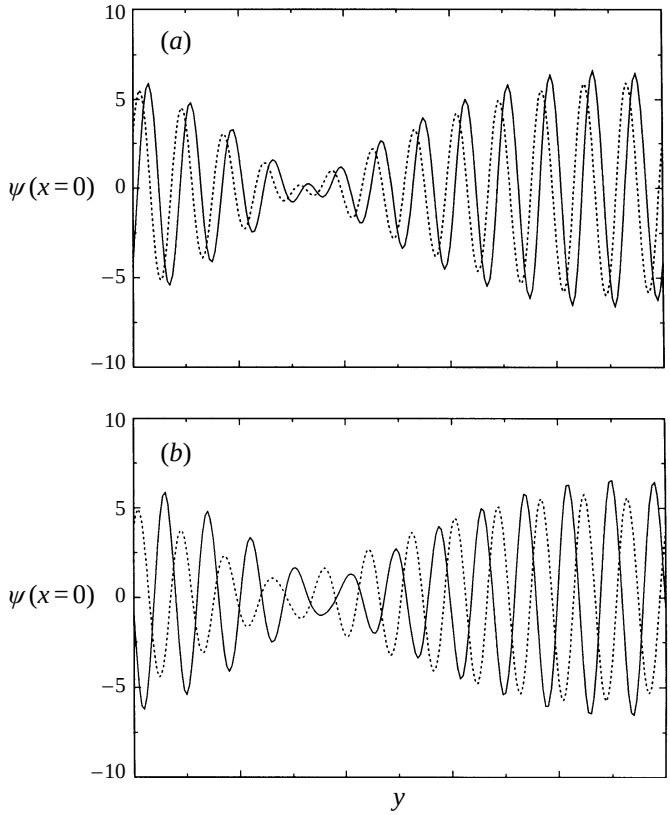

FIGURE 11. The stream function $\psi(0, y)$ for a particular instance of time in the case of modulated thermal Rossby waves computed with the full Galerkin method (solid lines) and with the GCGLE for $P = 0.03, \eta = 4000, S = 30$ and $R = 1495$ (a) and $R = 1500$ (b). The dashed lines have been obtained by multiplication of the envelope solution (6.1) by $\exp\{\mathrm{i}\alpha_c y\}$. The values of R for the dashed lines exceed those mentioned above by 5.

supercritical value of the Rayleigh number and thus the value of R_R increases far beyond the neutral curve $R_0(\alpha)$ such that the onset of the resonance instability is preceded by the mean flow instability.

6. Modulated thermal Rossby waves

The symmetric thermal Rossby waves which are unstable with respect to sideband instabilities become transformed into modulated thermal Rossby waves. The latter can be described as solutions of the GCGLE as well as with the Galerkin representation (2.4). For the solution of (4.3) we use the ansatz

$$A(y,t) = \sum_{n=-N}^{N} a_n(t) \exp\{\mathrm{i}(nq + q_0)y\} \quad \text{with} \quad q \equiv \frac{2\pi}{S}, \tag{6.1}$$

where S is the periodicity interval and where q_0 is a small wavenumber to accommodate the difference between the basic wavenumber α of the thermal Rossby wave and its critical value α_c. A typical choice for S is 30 since this value is also accessible with the Galerkin ansatz (2.4). In figure 11 a comparison is shown between the solutions obtained by the two methods. The fact that the best comparison is obtained when

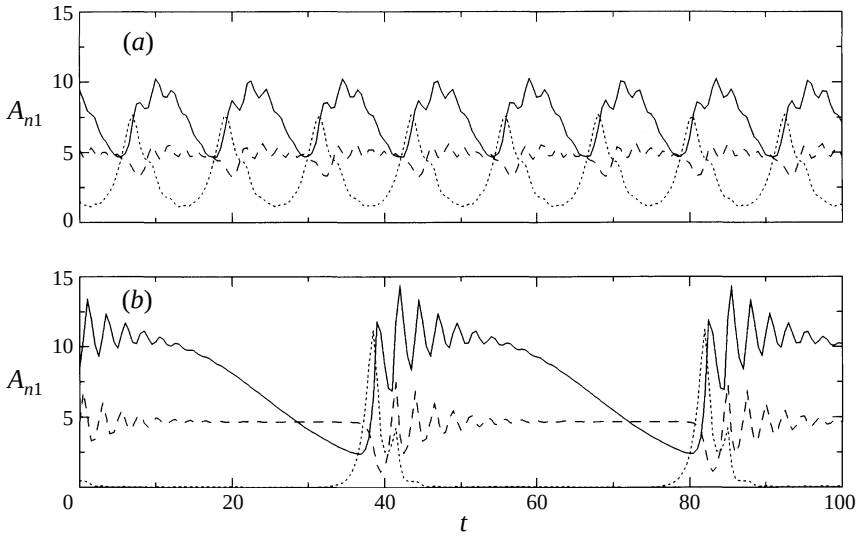

FIGURE 12. Time dependence of the amplitudes A_{41} (solid lines), A_{51} (dotted lines) and A_{91} (dashed lines) for the case $P = 0.03, \eta = 4000, S = 15$ and $R = 1680$ (*a*) and $R = 1710$ (*b*). The amplitudes A_{ln} are defined by $A_{ln} \equiv (\hat{a}_{ln}^2 + \check{a}_{ln}^2)^{1/2}$ based on the Galerkin representation (2.4) with $\alpha = 2\pi/S$.

the Rayleigh number in the GCGLE is increased by 5 can be attributed to the fact that the parabolic neutral curve of the GCGLE lies at somewhat higher values of R than $R_0(\alpha)$. The modulation corresponds to the excitation of two thermal Rossby waves with wavenumbers differing by q or $2q$ which propagate rather independently such that the modulation propagates with the group velocity $v_g = -\mathrm{d}\omega/\mathrm{d}\alpha$.

The relative simplicity of the GCGLE allows us to use much higher values of the periodicity interval. But no rules for the preferred wavelength of the envelopes have been found. In offering periodicity lengths S from 50 up to 300 it was found that usually the modulation wavelength corresponds to the periodicity interval S, but nearly as often an envelope with several wavelengths in the periodicity interval is realized. It obviously depends on initial conditions which kind of solutions of the form (6.1) is assumed. In general it is found that the dominant wavenumbers in the Galerkin solutions as well as in GCGLE solutions of the form (6.1) follow the left-hand branch of the neutral curve as the Rayleigh number is increased. As the Rayleigh number is increased further, the similarity between solutions of the Galerkin scheme and of the GCGLE disappears. More coefficients in the representation (2.4) participate in the dynamics and a complex periodic time dependence develops which does not lead to chaotic solutions, however. Two examples of those solutions are shown in figure 12.

The evolution of the streamline pattern with increasing R from the simply modulated thermal Rossby waves at $R = 1500$ to more complex time-dependent structures can be seen in figure 13. The increase with R of the average wavelength is noticeable and even the return to a periodic pattern of symmetric thermal Rossby waves can be observed in the last plot of the figure. Such simple solutions may be unstable, however, if the periodicity interval S is increased.

Although the ordinary CGLE as given by (4.1) is known to have chaotic solutions, such solutions have not been obtained from the GCGLE (4.3) in the low-Prandtl-number regime of interest in the present analysis. The fourth-order term on the

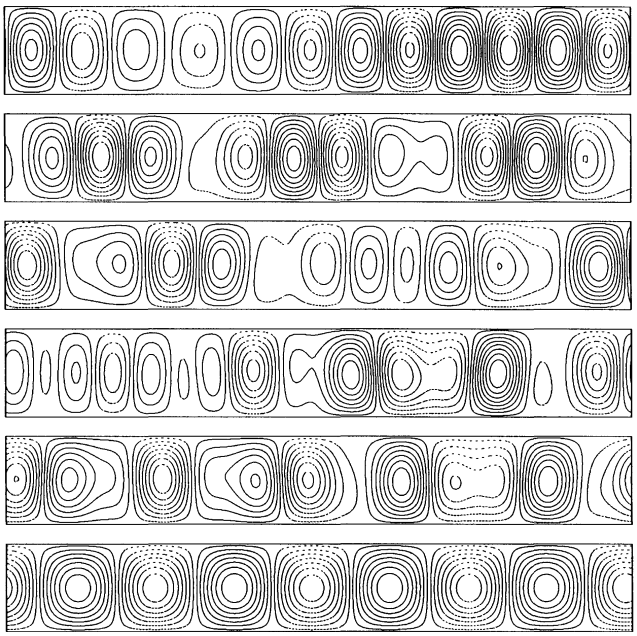

FIGURE 13. Instantaneous plots of the streamlines $\psi(x, y, t) = \text{const.}$ for the case $P = 0.03, \eta = 4000, S = 15$ for $R = 1500, 1560, 1620, 1680, 1740, 1800$ (from top to bottom).

right-hand side of (4.3) apparently changes the qualitative properties of the solutions as long as it is comparable to the preceding term.

7. Evolution of the resonance instability

In the case of the resonance instability it is also possible to follow the evolution of the bifurcating solution with a simpler system of equations than that obtained on the basis of the full Galerkin representation (2.4) for an appropriately extended periodicity interval in the y-direction. The mechanism of the instability suggests the consideration of three coupled amplitude equations

$$\frac{\mathrm{d}}{\mathrm{d}t}A_1 = (\sigma_0(R,\alpha) - \mathrm{i}\omega_1 + \sum_{j=1}^{3} c_{1j} \mid A_j \mid^2)A_1 + r_1 A_2 A_3, \tag{7.1a}$$

$$\frac{\mathrm{d}}{\mathrm{d}t}A_2 = (\sigma_0(R,d) - \mathrm{i}\omega_2 + \sum_{j=1}^{3} c_{2j} \mid A_j \mid^2)A_2 + r_2 A_1 A_3^*, \tag{7.1b}$$

$$\frac{\mathrm{d}}{\mathrm{d}t}A_3 = (\sigma^{(2)}(R,\alpha - d) - \mathrm{i}(\omega_1 - \omega_2) + \sum_{j=1}^{3} c_{3j} \mid A_j \mid^2)A_3 + r_3 A_1 A_2^*, \tag{7.1c}$$

corresponding to a solution of the form

$$\begin{aligned}\psi(x,y,t) = {} & [A_1(t)\exp\{\mathrm{i}\alpha y + \mathrm{i}\omega_1 t\} + A_2(t)\exp\{\mathrm{i}dy + \mathrm{i}\omega_2 t\}]\sin\pi(x+\tfrac{1}{2}) \\ & + A_3(t)\exp\{\mathrm{i}(\alpha - d)y + \mathrm{i}(\omega_1 - \omega_2)t\}\sin 2\pi(x+\tfrac{1}{2}) + \text{c.c.} + \text{h.o.t.}\end{aligned} \tag{7.2}$$

where the definitions (5.1d) and (5.2) have been used. The coefficients c_{ij} and r_i, $i, j = 1, 2, 3$, involve lengthy expressions and will not be given here explicitly. In

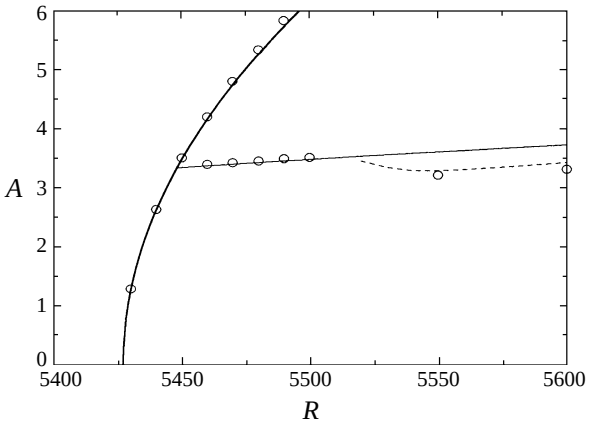

FIGURE 14. The amplitude $A \equiv 2(\sum |A_i|^2)^{1/2}$ derived from the 3-mode system (7.1) as a function of R for $P = 0.1, \eta = 4000, \alpha = 5.4, d = 0.54$. The thick solid line indicates periodic thermal Rossby waves, $A_2 = A_3 = 0$. The thin solid line denotes modulated thermal Rossby waves with a steady value of A and the dashed line indicates the time average of A for the vacillation state. Circles indicate solutions obtained from the full Galerkin scheme.

the actual calculation the functions σ_0 and $\sigma^{(2)}$ have been replaced by their Taylor expansion

$$\sigma_0(R, \alpha) = \sigma_0(R_0(\alpha), \alpha) + \left.\frac{\partial \sigma_0}{\partial R}\right|_{R_0,\alpha} (R - R_0(\alpha)), \tag{7.3a}$$

$$\sigma_0(R, d) = \sigma_0(R_0(\alpha), d) + \left.\frac{\partial \sigma_0}{\partial R}\right|_{R_0(\alpha),d} (R - R_0(\alpha)), \tag{7.3b}$$

$$\sigma^{(2)}(R, \alpha - d) = \sigma^{(2)}(R_0(\alpha), \alpha - d) + \left.\frac{\partial \sigma^{(2)}}{\partial R}\right|_{R_0(\alpha),\alpha-d} (R - R_0(\alpha)). \tag{7.3c}$$

The three coupled equations (7.1) can be justified rigorously only at a codimension-3 point of the system from which the actual calculations are far removed if such a point exists at all. The strongest deviation must be expected in the case of the third mode described by the amplitude $A_3(t)$. For large values of η the relative differences between the lowest Rayleigh numbers of modes proportional to $\sin \pi(x + \frac{1}{2})$ and $\sin 2\pi(x + \frac{1}{2})$ tend to vanish, however, as has been discussed by Busse (1986). It thus can be expected that the approximation provided by the system (7.1) will improve with increasing η. For a general discussion of amplitude equations describing the interaction of three resonating waves we refer to the book by Craik (1985).

As an example of the evolution of the resonance instability we consider the case of $d = 0.54, \alpha = 5.4$ for $P = 0.1, \eta = 4000$ which can easily be solved in the case of the full Galerkin representation (2.4) and with the three coupled amplitude equations (7.1). The results show rather close agreement as can be seen from the comparison shown in the bifurcation diagram of figure 14. From the onset of the resonance instability at $R_R = 5450$ up to $R_v = 5517$ the amplitudes $|A_n(t)|$ remain constant in time and describe a modulated thermal Rossby wave. At $R = R_v$ this stationary mixed solution becomes unstable to the onset of oscillations which we call amplitude vacillations because of their similarity with the vacillations found at higher Prandtl numbers (Schnaubelt & Busse 1992). As must be expected there are some slight quantitative differences between the calculations based on the 3-mode system (7.1) and the full

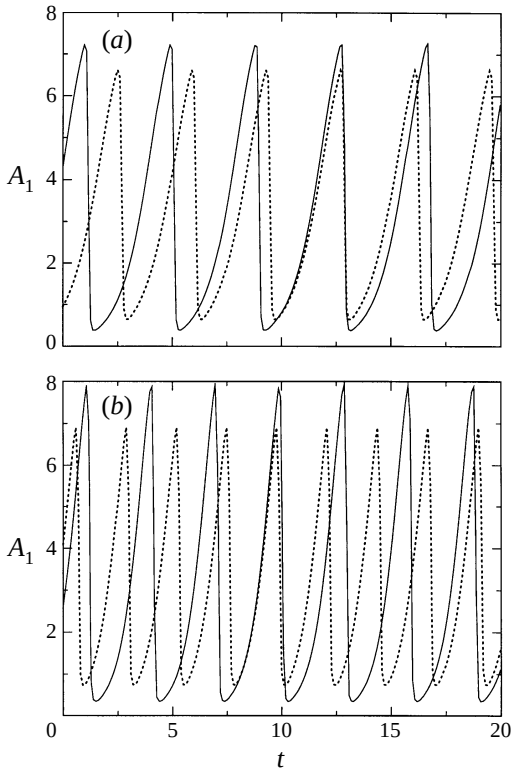

FIGURE 15. The amplitude A_1 (dashed line) derived from the 3-mode system (7.1) and the corresponding amplitude $A_{10,1} \equiv (\tilde{a}_{10,1}^2 + \tilde{a}_{10,1}^2)^{1/2}$ of the full Galerkin solution as a function of time for $P = 0.1, \eta = 4000, \alpha = 5.4, d = 0.54$ and $R = 5550$ (a) and $R = 5600$ (b).

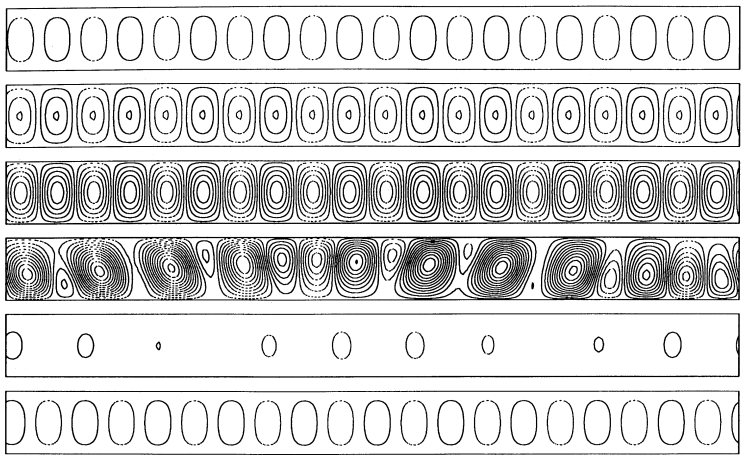

FIGURE 16. Plots of streamlines $\psi(x, y, t) = \text{const.}$ at equidistant times, 0.588 apart, (from top to bottom) obtained from time integrations with the Galerkin representation (2.4) with $\alpha = 0.54$ in the case $\eta = 4000, P = 0.1, R = 5600$. The dominant mode of convection corresponds to $\alpha_1 = 5.4$.

η	α_c	R_c	R_R	R_v	$R_R - R_c$	$R_v - R_c$
3000	4.72	3805	3825	3883	20	78
4000	5.40	5427	5448	5510	21	83
5000	5.97	7185	7206	7270	21	85
6000	6.45	9058	9080	9145	22	87
7000	6.88	11034	11056	11122	22	88
8000	7.26	13102	13125	13191	23	89
9000	7.62	15254	15277	15344	23	90
10000	7.94	17483	17507	17574	24	91

TABLE 1. Critical Rayleigh numbers R_c (onset of convection), R_R (onset of resonance instability), and R_v (onset of vacillation) at the critical value α_c of the wavenumber for different values η for the case $P = 0.1$

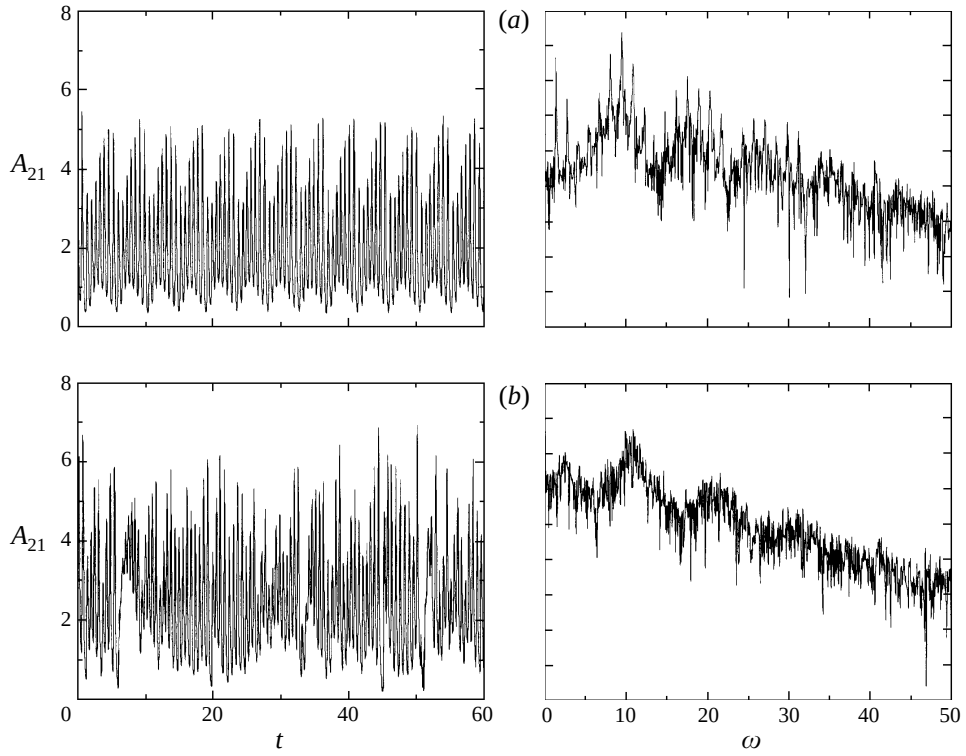

FIGURE 17. The amplitude $A_{21} \equiv (\hat{a}_{21}^2 + \check{a}_{21}^2)^{1/2}$ as a function of time for $P = 0.1, \eta = 4000, R = 6125$ (a) and $R = 6300$ (b). The aspect ratio S equals 30 corresponding to $\alpha = \pi/15$ in the representation (2.4). A logarithmic scale is used for the spectrum plotted on the right-hand side of the time series.

numerical solutions as shown in figure 15. But apart from these differences in the frequency and amplitude of vacillation there can be no doubt that both solutions describe the same phenomenon. To visualize the time dependence of the convection flow in real space a time sequence of plots of the stream function ψ is shown in figure 16 covering one period of oscillation. The growth of amplitude of the basic convection mode corresponding to $A_1(t)$ in (7.2) and the subsequent growth of the

modulation amplitude $A_2(t)$ followed by a rather sudden collapse of the convection flow are clearly evident from the figure.

The dependence of the transition Rayleigh numbers R_R and R_v on η is apparent from table 1. Although the critical wavenumbers α_c and the magnitudes of the Rayleigh numbers vary strongly, the differences $R_R - R_c$ and $R_v - R_c$ show only a slight change indicating that the onset of instabilities depends primarily on the amplitude of convection for fixed P.

As already apparent from figure 15, the differences between the 3-mode approach (7.1) and the full numerical treatment of the problem become larger with increasing Rayleigh number and the similarity between the two types of approximate solutions diminishes as new instabilities occur which introduce new frequencies into the time dependence. The numerical integration in time based on the Galerkin scheme (2.4) with the periodicity interval $S = 30$ show a transition to a chaotic time dependence as shown in figure 17. The vacillation frequency in the neighbourhood of $\omega \approx 10$ is still dominant in the spectrum of the time records shown in the figure. But at even higher Rayleigh numbers structures in the spectrum tend to disappear.

8. Concluding remarks

The analysis of this paper shows that a rich variety of dynamical features characterize convection in a rotating cylindrical annulus at low Prandtl numbers. Because of the large parameter space of the problem only some typical examples corresponding to relatively low Rayleigh numbers could be demonstrated in the preceding sections. A few more details can be found in chapter 3 of Herrmann (1996). Features that can be described on the basis of simpler equations than the full equations of motion have been emphasized. On the one hand the problem treated in this paper may serve as a physically realistic case for the application of envelope equations such as the CGLE and modifications thereof. On the other hand the dynamical behaviour of convection flows described by simple equations will be useful in the interpretation of results from numerical simulations of convection in rotating spherical fluid shells.

It is possible to realize low-Prandtl-number convection in a cylindrical annulus in a laboratory experiment. In fact, Azouni, Bolton & Busse (1986) have used mercury in such an experiment, but the measuring devices in their apparatus were not sophisticated enough to convey a good impression of the time-dependent dynamics of the convection columns. Unfortunately, it is not easy to visualize convection flows in low-Prandtl-number fluids such as mercury or other liquid metals. But with the new results reported in this paper it should be possible to design measuring methods which allow one to distinguish between the different dynamical regimes.

The nonlinear dynamics that can be studied in the annulus convection problem in a two-dimensional setting represents the simplest form of the dynamics that are expected in rotating self-gravitating fluid spheres. From experimental observations (see the review of Busse 1994) it is quite clear that the convection retains its approximately two-dimensional structure far into the turbulent regime. There is thus no doubt that the annulus problem will provide valuable insights into important questions such as the generation of mean zonal flows by convection and the dependence of the heat transport on the external parameters as regimes of high Rayleigh number are reached. Such insights will be especially important in the case of low-Prandtl-number fluids which are of primary interest for planetary and stellar applications.

REFERENCES

Azouni, A., Bolton, E. W. & Busse, F. H. 1986 Experimental study of convection columns in a rotating cylindrical annulus. *Geophys. Astrophys. Fluid Dyn.* **34**, 301–317.

Brummell, N. H. & Hart, J. E. 1993 High Rayleigh number β-convection. *Geophys. Astrophys. Fluid Dyn.* **68**, 133–150.

Busse, F. H. 1970 Thermal instabilities in rapidly rotating systems. *J. Fluid Mech.* **44**, 441–460.

Busse, F. H. 1986 Asymptotic theory of convection in a rotating, cylindrical annulus. *J. Fluid Mech.* **173**, 545–556.

Busse, F. H. 1994 Convection driven zonal flows and vortices in the major planets. *CHAOS* **4**, 123–134.

Busse, F. H. & Or, A. C. 1986 Convection in a rotating cylindrical annulus. Part 1. Thermal Rossby waves. *J. Fluid Mech.* **166**, 173–187.

Craik, A. D. D. 1985 *Wave Interactions and Fluid Flows.* Cambridge University Press.

Cross, M. C. & Hohenberg, P. C. 1993 Pattern formation outside of equilibrium. *Rev. Mod. Phys.* **65**, 851–1112.

Herrmann, J. 1996 Untersuchungen zur Konvektion im rotierenden Annulus bei kleinen Prandtlzahlen und bei modulierten Rändern. Dissertation, University of Bayreuth.

Herrmann, J. & Busse, F. H. 1994 Time dependent convection induced by centrifugal buoyancy in low Prandtl number fluids. In *Nonlinear Coherent Structures in Physics and Biology* (ed. K.-H. Spatschek & F. G. Mertens), pp. 401–404. Plenum.

Newell, A. C. 1974 Envelope equations. *Lect. Appl. Maths* **15**, 157–163.

Or, A. C. 1990 New phenomena in the Eckhaus instability of thermal Rossby waves. *J. Fluid Mech.* **216**, 613–628.

Or, A. C. & Busse, F. H. 1987 Convection in a rotating cylindrical annulus. Part 2. Transitions to asymmetric and vacillating flow. *J. Fluid Mech.* **174**, 313–326.

Or, A. C. & Herrmann, J. 1995 Anomalous sideband instabilities of thermal Rossby waves at low Prandtl numbers. *Phys. Fluids* A **7**, 315–323.

Schnaubelt, M. & Busse, F. H. 1992 Convection in a rotating cylindrical annulus. Part 3. Vacillating and spatially modulated flows. *J. Fluid Mech.* **245**, 155–173.